

Research Paper

Linear and Nonlinear Optical Properties in CdSe/ZnS/CdSe and ZnS/CdSe/ZnS Spherical Core-Shell-Shell Quantum Dots

Abdolali Rabanian¹, Mina Neghabi^{1*}, Mehdi Zadsar¹, Mostafa Jafari²

1. Department of Physics, Najafabad Branch, Islamic Azad University, Najafabad, Iran.

2. Department of Mathematics, Najafabad Branch, Islamic Azad University, Najafabad, Iran.

ARTICLE INFO

Article history:

Received 7 August 2023

Accepted 24 October 2023

Available online 1 February 2023

Keywords:

Spherical quantum dot

Nonlinear susceptibility

Absorption coefficient

Impurity.

ABSTRACT

In this work, we analyze and compare the optical properties of spherical A: CdSe–ZnS–CdSe and B: ZnS–CdSe–ZnS core–shell–shell quantum dots (CSQDs). Under the framework of the effective mass envelope function theory, the nonlinear susceptibilities associated with inter-sub-band transitions in the conduction band are computed by solving the three-dimensional Schrödinger equation for A and B QDs in the presence of impurity. We theoretically investigate the third-order susceptibilities and optical absorption coefficients as a function of core radius while the outer radius of quantum dots was fixed. The numerical calculations show that QD size plays a fundamental role in determining the nonlinear optical properties of QDs. The susceptibilities and the absorption coefficients have pronounced single peaks (resonance) and depend strongly on the geometry of these two quantum dots as well as the effect of the quantum confinement. Our theoretical study shows that susceptibility and absorption coefficients peaks are red-shifted by increasing the core radius, and the magnitude of susceptibility and absorption coefficient increase. The resonant magnitudes $\text{Im}(\chi^{(3)})$ of A and B-CSQD are negative and are around (-2.4) and (-2.5), respectively. While, for the core radius of $R_1 = 40$ nm, Real $(\chi^{(3)})$ of A and B-CSQD changes significantly near the resonant frequency from positive value (+1.7, +1.6) to negative one (-1.7, -1.6), respectively. Furthermore, for $R_1 = 40$ nm, the absorption coefficient of A-CSQDs has reached a maximum with the magnitude of situated at approximately 0.02 eV. In contrast, this value is equal to for B-CSQD. Our computational results may open a new window in the development of QDs structures for application in optoelectronic devices.

Citation: Rabanian, A.; Neghabi, M.; Zadsar, M.; Jafari, M. (2023). Linear and Nonlinear Optical Properties in CdSe/ZnS/CdSe and ZnS/CdSe/ZnS Spherical Core-Shell-Shell Quantum Dots, Journal of Advanced Materials and Processing, 11 (1), 3-12. Dor: 20.1001.1.2322388.2023.11.1.1.1

Copyrights:

Copyright for this article is retained by the author (s), with publication rights granted to Journal of Advanced Materials and Processing. This is an open – access article distributed under the terms of the Creative Commons Attribution License (<http://creativecommons.org/licenses/by/4.0>), which permits unrestricted use, distribution and reproduction in any medium, provided the original work is properly cited.



*** Corresponding Author:**

E-Mail: Neghabi@iaun.ac.ir

1. Introduction

Since the mid-1990s, with the improvement of nanotechnology and nanomaterials, core shell quantum dots (CSQDs) have been widely used in a variety of electronic devices and applications such as light-emitting diodes [1-3], solar concentrators [4-6], lasers [7-9], single-electron transistors [10-12], quantum computing [13-15], single-photon sources [16-18], Second-Harmonic Generation [19-21] and medical imaging [22-24]. It is obvious that the determination of the linear and nonlinear optical properties of the CSQDs is also necessary due to their widespread use in these various electronic device applications. Because of the great importance of CSQDs as a class of quantum-confined structures with excellent linear and nonlinear optical properties, several theoretical studies were performed to better calculate the susceptibilities and absorption coefficients of CSQDs and the optoelectronic processes that occur in these structures. These studies have covered research in the CSQDs field, and many have focused on various aspects of the effect of the CSQD size [25], the applied potential [26], the impurity [27-29], and the external electromagnetic fields [30], on optical properties.

Many studies about optical properties have been studied and proposed. Zeiri et al., have calculated the third nonlinear optical susceptibility in CdTe–CdS–ZnS core–shell–shell quantum dots [31]. They theoretically investigate the third-order susceptibilities as a function of the core, shell radii, pump photo energy, and time relaxation. This study has revealed that CSQD size plays a fundamental role in determining the nonlinear optical properties of CSQDs. Naifar et al. have investigated the eigenvalues, transition energy, and the linear and nonlinear dielectric functions have been numerically investigated for CdS/ZnS spherical core/shell quantum dots embedded in various dielectric matrices [32]. Their evaluation was carried out for three commonly used matrices such as PVA, PMMA, and SiO₂. Calculations were done under the effective mass approximation and compact density matrix approach. Results revealed that the nonlinear optical property is strongly affected by the nature of the matrix material. By increasing the core/shell radii ratio, the energy states, as well as the transition energy, are decreasing. It is also indicated that the presence of the dielectric mismatch in the QD-matrix system can cause significant enhancement on the linear and third-order nonlinear dielectric function.

Ghosh et al. have inspected the role of binding energy (BE) on nonlinear optical properties of doped GaAs quantum dots [33]. The effects of dot size on energy levels, dipole transition matrix, and third-order nonlinear optical susceptibilities in a core/shell structure of CdS/ZnS spherical QD have been investigated by Hasanirokh et al. [34]. Their proposed structure shows the large dipole transition and high nonlinear and tunable susceptibilities that are very suitable for the implementation of active and passive devices. A detailed investigation of the effect of core and shell radii on the energies and the dielectric function of GaN/Al_xGa_{1-x}N quantum dots has been exhibited by Zeiri et al. [35]. Their numerical results indicate that by increasing radii, the dielectric function shifts to lower frequencies, and by increasing the value of the quantum dots density, the peaks of the dielectric function are redshifted, and the intensities increase as a function of the pump photon energy. Vahdani et al. have demonstrated the linear and nonlinear optical dielectric function of a slab of CdSe/ZnS quantum dot matrix associated with intersubband transitions [36]. Their results show that the behavior of third-order nonlinear susceptibility is similar to the dielectric function of QDs.

In this paper, we study two core/shell/shell spherical quantum dot heterostructures of A: CdSe/ZnS/CdSe and B: ZnS/CdSe/ZnS for cases with and without a center impurity. In the structure of A, the band gap of the core is smaller than the band gap of the shell. While the core is encapsulated with a shell that has a larger band gap in the structure of B. We compare the optical properties of these two structures and report the detailed calculation of the third-order susceptibilities and the absorption coefficients. Since the ZnS band gap as core (shell) is much larger than that of CdSe as shell (core), it is expected that the optical properties of these two structures will be different.

2. Theory and calculation

We consider two spherical core/shell/shell quantum dots in the structures of A: CdSe/ZnS/CdSe and B: ZnS/CdSe/ZnS. We assumed that the structure of A is composed of CdSe core and ZnS and CdSe shells. While, the core of the structure of B is ZnS, which is enveloped by the CdSe and ZnS shells. However, both the A and B structures have cores with inner radius R_1 and shells with R_2 and R_3 radii, as shown in Fig. 1. It is seen that these structures are defined as one-step infinity quantum dots.

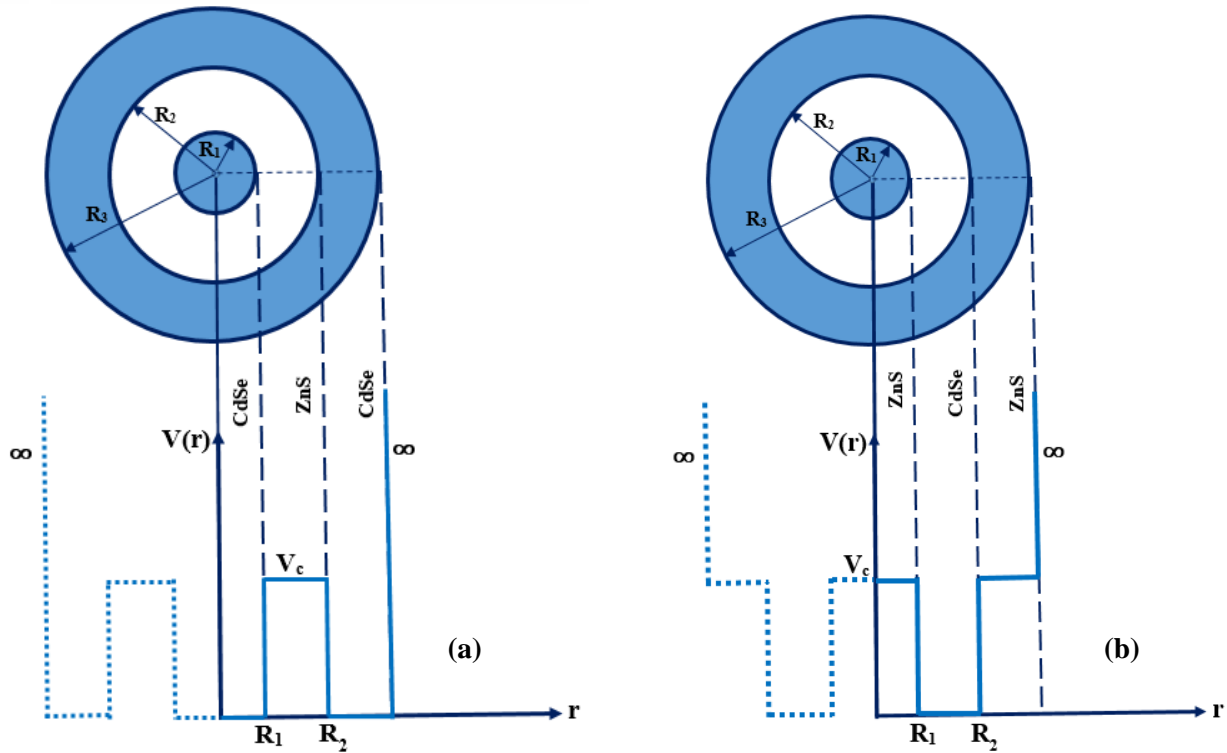


Fig. 1. Schematic illustration of spherical core/shell/shell quantum dot (a) CdSe/ZnS/CdSe and (b) ZnS/CdSe/ZnS and their potential profile. The radii of core, shell1 and shell2 are R_1 , R_2 and R_3 , respectively.

We use the numerical method in the framework of the effective mass approximation to simulate the A and B QDs, which are assumed to have perfect spherical symmetry.

The Hamiltonian of an electron confined in each of A and B QDs in the presence of on-center hydrogenic impurity can be described as:

$$H = H_0 + U(r) \quad \text{where} \quad H_0 = -\frac{\hbar^2}{2m_i^*} \nabla^2 + V_0(r) \quad (1)$$

where H_0 and $U(r)$ denote the Hamiltonian of an electron and the Coulomb interaction of the electron with the impurity in a nonuniform dielectric medium, respectively. Also, the effective mass (m_i^*) and the confinement potential ($V_0(r)$) both depend on the electron position in the hetero-structure.

The radial Schrödinger equation is used to find the eigenfunctions ($R_{n,l}(r)$) of the Hamiltonian with spherical symmetry in Eq. (1) and their corresponding energies E , so that it can be written as:

$$\left\{ -\frac{\hbar^2}{2m_i^*} \left[\frac{d^2}{dr^2} + \frac{2}{r} \frac{d}{dr} - \frac{l(l+1)}{r^2} \right] + V(r) + U(r) \right\} R_{n,l} = E_{n,l} R_{n,l} \quad (2)$$

In order to achieve reasonable expressions of the eigenenergies and their corresponding wave functions, the continuity conditions at all boundaries of the studied A and B QDs must be satisfied as follows:

$$\begin{cases} R_{n,l}(r_i) = R_{n,l}(r_{i+1}) \Big|_{r=r_i} \\ \frac{1}{m_i^*} \frac{dR_{n,l}(r_i)}{dr} = \frac{1}{m_{i+1}^*} \frac{dR_{n,l}(r_{i+1})}{dr} \Big|_{r=r_i} \end{cases} \quad (3)$$

The expression of the first and third-order nonlinear optical susceptibility for two energy levels, the ground and the first excited states, is given by [35,36]:

$$\chi^{(1)}(\omega) = \frac{\sigma_v |M_{21}|^2}{E_{21} - \hbar\omega - i\hbar\Gamma} \quad (4)$$

$$\chi^{(3)}(\omega) = \frac{\sigma_v |M_{21}|^2}{E_{21} - \hbar\omega - i\hbar\Gamma} \left[\frac{4|M_{21}|^2}{(E_{21} - \hbar\omega)^2 + (\hbar\Gamma_{12})^2} - \frac{(M_{22} - M_{11})^2}{(E_{21} - i\hbar\Gamma_{12})(E_{21} - \hbar\omega - i\hbar\Gamma_{12})} \right] \quad (5)$$

where σ_v represents the carrier density, $E_{ij} = E_i - E_j$ is the energy difference between the two states and $M_{21} = |\langle R_i | er | R_j \rangle|$ which is the transversal part. In our calculations, the relation between the optical intensity and the applied electric field is taken from Ref. [37].

In order to investigate the linear and nonlinear absorption coefficients which are related to the corresponding electric susceptibility, we have used the expression taken from Ref. [37]:

$$\alpha(\omega) = \omega \sqrt{\frac{\mu}{\epsilon_r}} \text{Im}(\epsilon_0 \chi(\omega)) \quad (6)$$

Then, the linear and third-order nonlinear dielectric functions can be expressed as:

$$\alpha^{(1)}(\omega) = \omega \sqrt{\frac{\mu}{\epsilon_r}} \frac{\sigma_v \hbar \Gamma_{ij} |M_{ij}|^2}{(E_j - E_i - \hbar\omega)^2 + (\hbar\Gamma_{ij})^2} \quad (7)$$

$$\alpha^{(3)}(\omega, I) = -\omega \sqrt{\frac{\mu}{\epsilon_r}} \left(\frac{I}{2\epsilon_0 n_r c} \right) \frac{4\sigma_v \hbar \Gamma_{ij} |M_{ij}|^4}{[(E_j - E_i - \hbar\omega)^2 + (\hbar\Gamma_{ij})^2]^2} \quad (8)$$

The total dielectric function of CSQDs is defined by the expression:

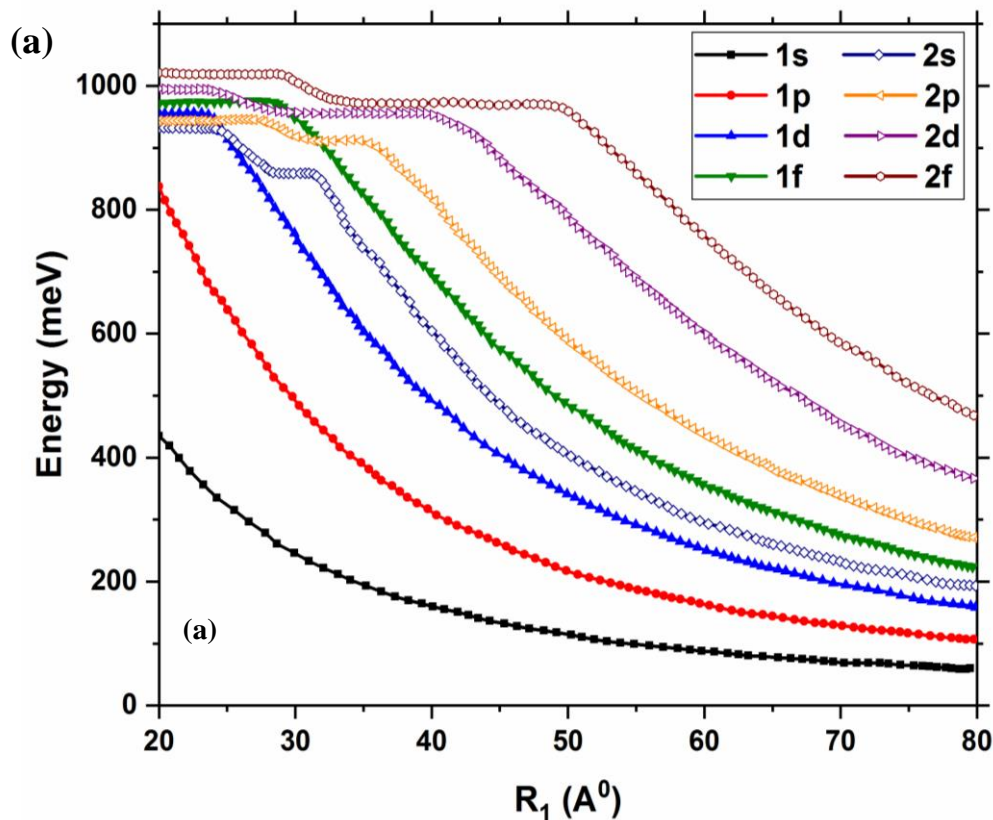
$$\alpha(\omega, I) = \alpha^{(1)}(\omega) + \alpha^{(3)}(\omega, I)$$

3. Numerical results

In our calculations, the following parameters are used: $m_{CdSe}^* = 0.13 m_0$, $m_{ZnS}^* = 0.28 m_0$, $E_{g\ CdSe} = 1.84\ eV$, $E_{g\ ZnS} = 3.54\ eV$, $\epsilon_{CdSe} = 9.56$, $\epsilon_{ZnS} = 3.54$ and $V_c = 900\ eV$ [38].

Considering the impurity at center of each of A and B spherical CSQDs, the single electron eigenenergies have been calculated for the s, p, d and f states. We have investigated the optical properties of the spherical CdSe/ZnS/CdSe and ZnS/CdSe/ZnS quantum dots in the case of the last shell radius R_2 is constant while the radius of the core sphere is varied. Remarkably, the energy levels of the electron for A and B CSQDs in this case are given as a function of the core radius R_1 increases to $80\ \text{\AA}$, where $R_2 = 150\ \text{\AA}$ is a fixed parameter in Fig. 2a and b. It is found that in the case of A CSQD, for the first (1s, 1p, 1d, and 1f) state energies, the eigenenergies are completely reduced as the size of the core increased for both 1s and 1p, indicating that electron-confined in the core and the effect of quantum confinement befalls on the electron. It should be noted that the Bohr radius for materials ZnS and CdSe are 2.5 and 5.6 nm, respectively [39]. When the size of the particle approaches exciton Bohr diameter, the

quantum confinement effect occurs, and the optical properties of CSQDs change drastically. While for 1d and 1f states, there is a steady trend first and then decreases. In fact, the electron confinement has not occurred for the small core radii and energies are almost constant up to $R_1 = 25\ \text{\AA}$ and $R_1 = 30\ \text{\AA}$ for 1d and 1f states, respectively. But when the core radius (R_1) increases, the electron confinement is relieved. On the other hand, the second (2s, 2p, 2d and 2f) state energies have a second flattening which indicates that the probability distribution will have two peaks. When the energies are on the second flattening, the second peak is outside the core, and this is because the size of the core is still insufficient to confine the second peak. However, it can be seen that this second peak penetrates into the core as the energy decreases uniformly. Fig. 2b shows that there is a sharp difference between the trends of energy changes in terms of R_1 for B-CSQD compared to A-CSQD. For B-CSQD, it is obvious that the eigenenergies have an increasing trend for all the first (1s-1f) and second (2s-2f) levels. However, the energy of the first states essentially is lower than that of the second states. The obvious reason for this increase is that in the B-CSQD, the electron is confined within the inner shell (CdSe) and can't penetrate the inner dot due to potential barrier applied by the ZnS core layer.



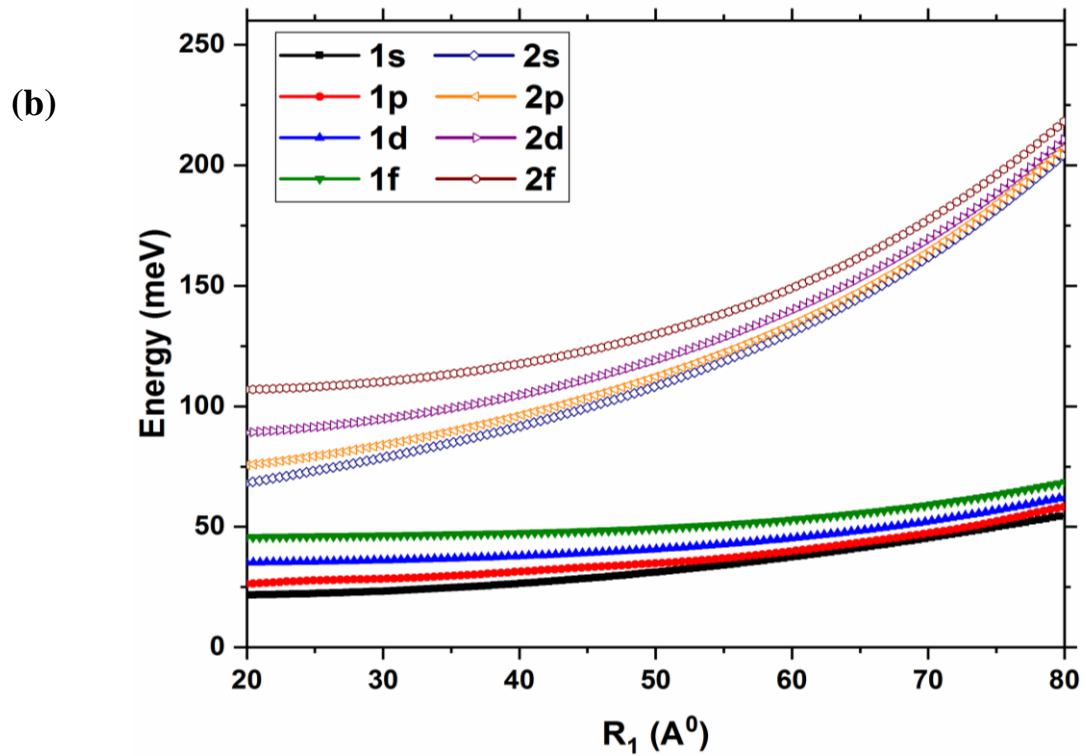


Fig. 2. Energy levels of (a) the spherical CdSe/ZnS/CdSe quantum dot and (b) the spherical ZnS/CdSe/ZnS quantum dot with the impurity as functions of the core radius for constant R_2 .

In Fig. 3(a,b) we have depicted the variation of the third-order susceptibility as a function of wavelength in the A-CSQD, for four different values of core radius (R_1) in both cases $E > V_c$ and $E < V_c$. From this figure we can see that increasing R_1 leads to a shift for the susceptibility peak towards the longer wavelength for both cases ($E > V_c$ and $E < V_c$). Both the magnitude of the peak and its position depend on the radius of the core. When the radius of the core increases, energy distances between electronic states become smaller. Therefore, the larger the size of the core, the smaller the energy distance, and the dipole matrix element (μ) becomes stronger by increasing the radius of the core. Also, Real and Imaginary part of susceptibility (Real ($\chi^{(3)}$) and Im ($\chi^{(3)}$)) of A-CSQD is shown in Fig. 3c when $E < V_c$, as a function

of wavelength at different core radius while the radius of the shell is fixed. One can notice that when R_1 increases, the peaks of Real ($\chi^{(3)}$) and Im ($\chi^{(3)}$) are enhanced and redshifted. According to Fig. 3(c), we can observe that for $R_1 = 40$ nm, the resonant magnitude Im ($\chi^{(3)}$) is negative and being around 2.4 while Real ($\chi^{(3)}$) changes significantly near the resonant frequency from positive value (+1.7) to negative one (-1.7). When the core radius of the quantum dot increases, the electron is confined in the core, and the effect of quantum confinement befalls the electron; thus, the dipole transition matrix element μ increases and this effect showed an improvement in the nonlinear optical properties. The result is in agreement with those of other researchers [40-42].

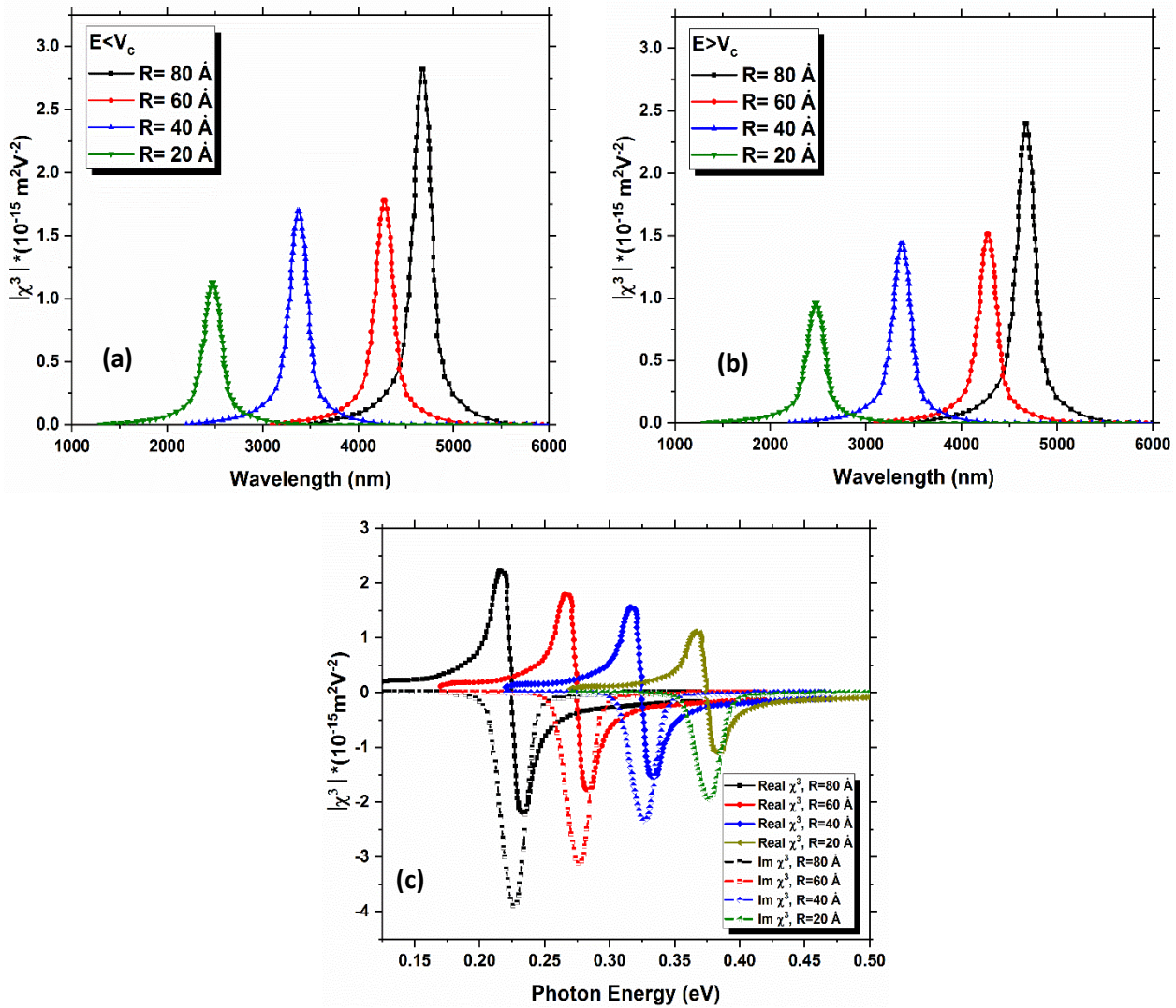


Fig. 3. (a,b) Modulus of susceptibility ($\chi^{(3)}$) for $E < V_c$ and $E > V_c$, as a function of wavelength, and (c) The real and imaginary part of susceptibility (Real ($\chi^{(3)}$) and Im ($\chi^{(3)}$)) when $E < V_c$, as a function of photon energy at different core radius.

In Fig. 4(a,b), the third-order susceptibility of B-CSQD has been displayed as a function of pump photon energy with four values of core radius in both cases $E < V_c$ and $E > V_c$. It is clear remark that for ZnS/CdSe/ZnS CSQD, the resonant magnitude of $\chi^{(3)}$ is about $1.7 \times 10^{-15} \frac{\text{m}^2}{\text{V}^2}$ for $R_1 = 40 \text{ nm}$ in the case $E < V_c$. Increasing R_1 leads to a shift of $\chi^{(3)}$ peak toward the longer wavelength for $E < V_c$ and $E > V_c$. Furthermore, both intensity and position of $\chi^{(3)}$ peaks depend on core radius, and this can be related to the quantum size effect in the conduction band. The resonant magnitude of $\chi^{(3)}$ in ZnS/CdSe/ZnS CSQD is around $1.3 \times 10^{-15} \frac{\text{m}^2}{\text{V}^2}$ in the case $E > V_c$. It may be worth pointing out for the case where $E > V_c$ that the intensities of the susceptibility peaks have very low values comparing with case $E < V_c$. In Fig. 4(c) the real and imaginary parts (Real ($\chi^{(3)}$) and Im ($\chi^{(3)}$)) of A-CSQD as a

function of the pump photon energy $\hbar\omega(\text{eV})$ for different values of R_1 have been shown when $E < V_c$. The plot reveals that Real ($\chi^{(3)}$) and Im ($\chi^{(3)}$) depend strongly on R_1 . We can see that, Real ($\chi^{(3)}$) and Im ($\chi^{(3)}$) increase when increasing core radius from 20 nm to 80 nm. In fact, for a chosen value $R_1 = 40 \text{ nm}$, Real ($\chi^{(3)}$) changes its signs from a negative value (-1.6) to a positive one (+1.6) while Im ($\chi^{(3)}$) ways keeps approximately a negative value in the vicinity of (-2.5). By increasing core radius, Real ($\chi^{(3)}$) and Im ($\chi^{(3)}$) both witness a progressive redshift. We can remember for this section that the positions and intensities of susceptibility's peaks depend on core radius value. By increasing the core radius from 20 nm to 80 nm, the probability of distribution of the electronic wave function is principally well confined, and so there is no electron distribution in the shells for $R_1 = 80 \text{ nm}$.

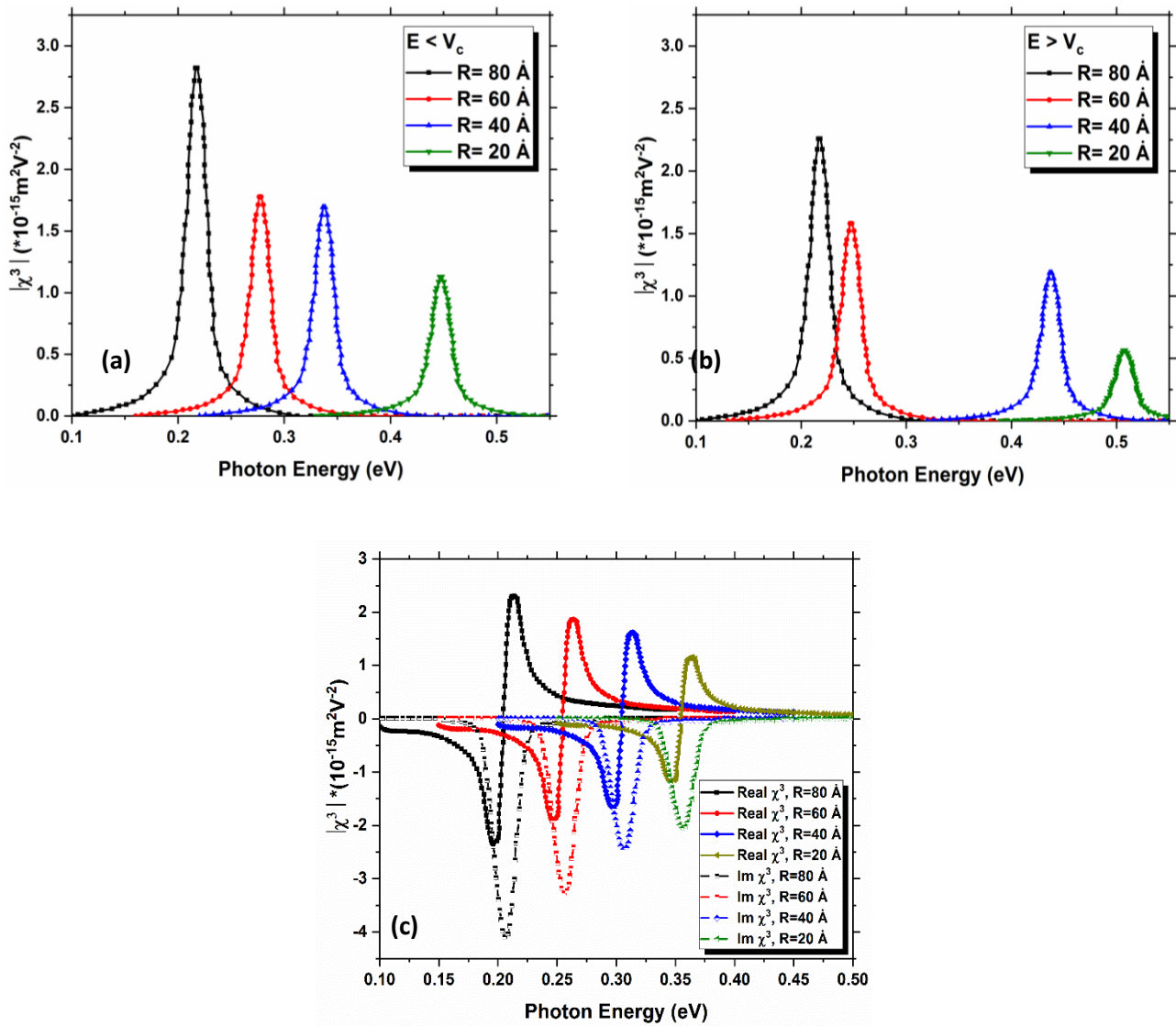


Fig. 4. (a,b). Modulus of susceptibility ($\chi^{(3)}$) for $E < V_c$ and $E > V_c$, **(c)** The real and imaginary part of susceptibility (Real ($\chi^{(3)}$) and Im ($\chi^{(3)}$)) when $E < V_c$, as a function of photon energy at different core radius

In Fig. 5(a,b), the imaginary parts of the linear and nonlinear absorption coefficient of A and B-CSQD have been plotted as a function of the pump photon energy $\hbar\omega$ (eV) for different values of R_1 with $I = 0.2$ MW/cm for $E < V_c$. The plots reveals that when increasing R_1 , a redshift of peaks appears. For $R_1 = 40$ nm, the absorption coefficient of A-CSQDs has reached a maximum with the magnitude of $0.7 \times$

10^{15}m^{-1} situated at approximately 0.02 eV. While this value is equal to $0.9 \times 10^{15} \text{m}^{-1}$ for B-CSQD. Therefore, the effect of geometry of these two CSQDs as well as the adjustment of size and material parameters can be a first step to achieve an enhancement of susceptibility and absorption coefficient that this behavior can be related to quantum confinement effects.

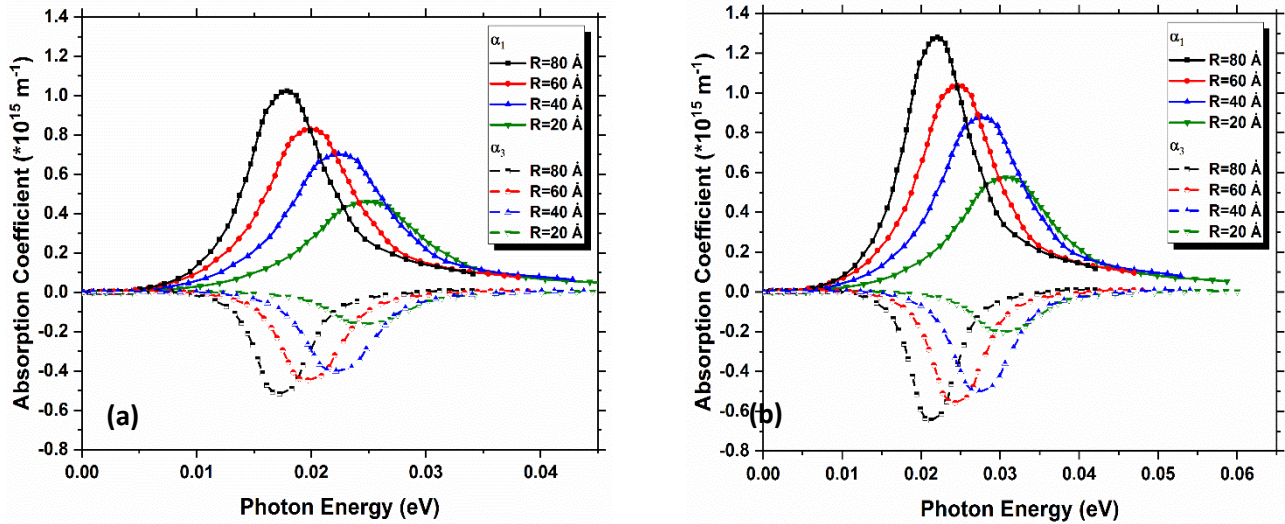


Fig. 5. (a and b). Linear and Nonlinear absorption coefficient of A and B-CSQD, as a function of photon energy at different core radius

4. Conclusions

We investigated the optical properties of two quantum dots with structures of A: CdSe/ZnS/CdSe and B: ZnS/CdSe/ZnS by using numerical modeling. The calculations were performed while the total radius of the quantum dot remained constant and the radius of the core (R_1) increased. It was found that the changes in core layer thickness can affect the third-order susceptibility and absorption coefficient of the A and B CSQDs. Calculations show that in A and B-CSQD, the third order nonlinearity susceptibility and the linear, nonlinear parts of the absorption coefficient depends strongly on the core radius R_1 . By increasing radius, we found that $(\chi^{(3)})$ and α shifts to lower energies. It is observed that in the case of CdSe/ZnS/CdSe CSQD for $R_1 = 40$ nm, the resonant magnitude $\text{Im}(\chi^{(3)})$ is -2.4 while $\text{Real}(\chi^{(3)})$ changes from value (+1.7) to one (-1.7). On the other hand, for ZnS/CdSe/ZnS CSQD, $\text{Real}(\chi^{(3)})$ changes from (-1.6) to (+1.6) while $\text{Im}(\chi^{(3)})$ ways keeps approximately a negative value in the vicinity of (-2.5). For ZnS/CdSe/ZnS CSQD, the resonant magnitude of $\chi^{(3)}$ is about $1.7 \times 10^{-15} \frac{m^2}{V^2}$ and $1.3 \times 10^{-15} \frac{m^2}{V^2}$ for $R_1 = 40$ nm in the case $E < V_c$ and $E > V_c$, respectively. Also, for $R_1 = 40$ nm, the absorption coefficient of A-CSQDs has reached a maximum $0.7 \times 10^{15} m^{-1}$ situated at approximately 0.02 eV. While this value is equal to $0.9 \times 10^{15} m^{-1}$ for B-CSQD. The result of this work can be utilized in the fabrication of optoelectronics and photonic devices such as radar-microwave absorbers and improved electrically small antenna.

Acknowledgment

Authors are thankful to the Islamic Azad University, Najafabad Branch Research Council for the partial support of this research.

References

- [1] Jin, X., et al., Thick-shell CdZnSe/ZnSe/ZnS quantum dots for bright white light-emitting diodes. *Journal of Luminescence*, 2020: p. 117670.
- [2] Deng, B., et al., Low temperature synthesis of highly bright green emission CuInS₂/ZnS quantum dots and its application in light-emitting diodes. *Journal of Alloys and Compounds*, 2020: p. 155400.
- [3] Ye, Y., et al., Efficient multi-shell CuInS₂/ZnS/ZnS quantum-dots based light-emitting diodes: Time-controlled synthesis of quantum-dots and carrier balance effects of PEI. *Optical Materials*, 2020. 106: p. 109926.
- [4] Ganguly, A. and S. Nath, Mn-doped CdS quantum dots as sensitizers in solar cells. *Materials Science and Engineering: B*, 2020. 255: p. 114532.
- [5] Wang, A., et al., Advances in perovskite quantum-dot solar cells. *Journal of Energy Chemistry*, 2020.
- [6] Latif, H., et al., A novel, PbS quantum dot-Sensitized solar cell structure with TiO₂-fMWCNTS nano-composite filled meso-porous anatase TiO₂ photoanode. *Solar Energy*, 2020. 204: p. 617-623.
- [7] Radzi, N., et al., Q-switched fiber laser based on CdS quantum dots as a saturable absorber. *Results in Physics*, 2020. 16: p. 103123.
- [8] Barseghyan, M., et al., Control of electronic and optical properties of a laser dressed double quantum dot molecule by lateral electric field. *Physica E: Low-dimensional Systems and Nanostructures*. 126: p. 114362.
- [9] Yousefvand, H.R., Impact of carrier heating on

- performance of quantum-dot semiconductor lasers: Theoretical study and circuit-level modeling. *Optics Communications*, 478: p. 126395.
- [10] Moulhim, A., B. Tripathi, and M. Kumar, Investigating the effect of quantized confining energy on the quantum coulomb blockade phenomena in single-electron transistor. *Solid State Communications*, 2020: p. 114078.
- [11] Ali, H., et al., Single-electron pumping in a ZnO single-nanobelt quantum dot transistor. *Science China Physics, Mechanics & Astronomy*, 2020. 63(6): p. 267811.
- [12] Khademhosseini, V., et al., Current Analysis of Single Electron Transistor Based on Graphene Double Quantum Dots. *ECS Journal of Solid State Science and Technology*, 2020. 9(2): p. 021003.
- [13] Hensen, B., et al., A silicon quantum-dot-coupled nuclear spin qubit. *Nature Nanotechnology*, 2020. 15(1): p. 13-17.
- [14] Kodera, T. Silicon quantum dot devices for spin-based quantum computing. in *2020 IEEE Silicon Nanoelectronics Workshop (SNW)*. 2020. IEEE.
- [15] Ricco, L., et al., Interaction induced hybridization of Majorana zero modes in a coupled quantum-dot–superconducting-nanowire hybrid system. *Physical Review B*, 2020. 102(16): p. 165104.
- [16] Ollivier, H., et al., Reproducibility of high-performance quantum dot single-photon sources. *ACS Photonics*, 2020. 7(4): p. 1050-1059.
- [17] Baride, A., et al., One-and two-photon electron-transfer induced uncaging of coumarin from cinnamate-capped CdSe quantum dots. *Journal of Luminescence*, 2020: p. 117112.
- [18] Kotb, A. and C. Guo, All-optical NOR and XNOR logic gates at 2 Tb/s based on two-photon absorption in quantum-dot semiconductor optical amplifiers. *Optical and Quantum Electronics*, 2020. 52(1): p. 30.
- [19] Makhlof, D., et al., Modeling of the second harmonic generation in a lens-shaped InAs/GaAs quantum core/shell dot under temperature, pressure and applied electric field effects. *Results in Physics*, 2020. 16: p. 102961.
- [20] Evangelou, S., Comment on “Tunneling effect on second-harmonic generation in quantum dot molecule, Superlattices and Microstructures 91 (2016) 358-364”. *Superlattices and Microstructures*, 2020: p. 106708.
- [21] Arif, S., et al., Analyzing role of relaxation time on second harmonic generation and optical dielectric function of impurity doped quantum dots under the aegis of noise. *Physica B: Condensed Matter*, 2020: p. 412166.
- [22] Kashani, H.M., et al., Bottom-up and green-synthesis route of amino functionalized graphene quantum dot as a novel biocompatible and label-free fluorescence probe for in vitro cellular imaging of human ACHN cell lines. *Materials Science and Engineering: B*, 2019. 251: p. 114452.
- [23] Rana, M., et al., Glutathione capped core/shell CdSeS/ZnS quantum dots as a medical imaging tool for cancer cells. *Inorganic Chemistry Communications*, 2020. 112: p. 107723.
- [24] Liang, H., et al., Carbon quantum Dot@ Silver nanocomposite–based fluorescent imaging of intracellular superoxide anion. *Microchimica Acta*, 2020. 187(9): p. 1-9.
- [25] Vinasco, J.A., et al., Effects of Geometry on the Electronic Properties of Semiconductor Elliptical Quantum Rings. *Scientific Reports*, 2018. 8(1): p. 13299.
- [26] Khordad, R., B. Mirhosseini, and M.M. Mirhosseini, Thermodynamic Properties of a GaAs Quantum Dot with an Effective-Parabolic Potential: Theory and Simulation. *Journal of Low Temperature Physics*, 2019. 197(1): p. 95-110.
- [27] Akankan, O., et al., The effects of geometrical shape and impurity position on the self-polarization of a donor impurity in an infinite GaAs/AlAs tetragonal quantum dot. *Indian Journal of Physics*, 2020.
- [28] Stevanović, L., et al., Theoretical investigation of the transient regime of electromagnetically induced transparency in spherical quantum dot with on-center hydrogen impurity. *Optical and Quantum Electronics*, 2020. 52(3): p. 1-10.
- [29] Akankan, O., et al., The effects of geometrical shape and impurity position on the self-polarization of a donor impurity in an infinite GaAs/AlAs tetragonal quantum dot. *Indian Journal of Physics*, 2020: p. 1-4.
- [30] Osorio, J.A., et al., Pyramidal core-shell quantum dot under applied electric and magnetic fields. *Scientific Reports*, 2020. 10(1): p. 8961.
- [31] Zeiri, N., et al., Theoretical studies on third nonlinear optical susceptibility in CdTe–CdS–ZnS core–shell–shell quantum dots. *Photonics and Nanostructures - Fundamentals and Applications* 36 (2019) 100725.
- [32] Naifar, A., et al., Dielectric environment effect on linear and nonlinear optical properties for CdS/ZnS core/shell quantum dots. *Results in Physics*, 2019. 14: p. 102513.
- [33] Ghosh, A.P., et al., Influence of position-dependent effective mass on the nonlinear optical properties of impurity doped quantum dots in presence of Gaussian white noise. *Optics Communications*, 2016. 367: p. 325-334.
- [34] Hasanirokh, K., A. Asgari, and M.M. Rokhi, Theoretical study on nonlinear optical properties of CdS/ZnS spherical quantum dots. *Optik*, 2019. 188: p. 99-103.
- [35] Zeiri, N., et al., Theoretical investigation on linear

- and nonlinear dielectric function for GaN/Al_xGa_{1-x}N core/shell quantum dots. *Materials Science and Engineering: B*, 2020. 261: p. 114675.
- [36] Vahdani, M. and N. Ehsanfard, Nonlinear optical properties of a slab of CdSe/ZnS quantum dot matrix. *Physica B: Condensed Matter*, 2018. 548: p. 1-9.
- [37] Mathe, L., et al., Linear and nonlinear optical properties in spherical quantum dots: Inversely quadratic Hellmann potential. *Physics Letters A*, 2021. 379: p. 1-10.
- [38] Stojanović, D. and R. Kostić, Hydrogenic impurity states in the spherical CdSe/ZnS/CdSe nanoheterostructure. *Optical and Quantum Electronics*, 2016. 48(4): p. 226.
- [39] I. Gerdova and A. Hach, Third-order non-linear spectroscopy of CdSe and CdSe/ZnS core shell quantum dots. *Optics Communications*, 2005. 243: p. 205-212.
- [40] A. Sabah., et al., Investigation of band parameters and electrochemical analysis of multi core-shell CdSe/CdS/ZnS quantum dots. *Optical Materials*, 2023. 142: p. 114065.
- [41] M. Hu., et al., A fluorescent lateral flow immunoassay based on CdSe/CdS/ZnS quantum dots for sensitive detection of olaquinox in feedstuff. *Food Chemistry*, 2023. 419: p. 136025.
- [42] X. Cao., et al., High-performance luminescent solar concentrators based on the core/shell CdSe/ZnS quantum dots composed into thiol-ene polymer. *Journal of Luminescence*, 2022. 252: p. 119368.